Systematic studies of terahertz metamaterials fabricated on thin Mylar film

Jianqiang Gu (谷建强)[1,2*], Changlei Wang (王昌雷)[1], Zhen Tian (田 震)[1,2], Feng Liu (刘 丰)[1], Xueqian Zhang (张学迁)[1], Jiaguang Han (韩家广)[1], Mingxia He (何明霞)[1], Qirong Xing (邢岐荣)[1], Weili Zhang (张伟力)[1,2], Lu Chai (柴 路)[1], and Qingyue Wang (王清月)[1]

[1] *Center for Terahertz Waves and College of Precision Instrument and Optoelectronics Engineering, Tianjin University, Tianjin 300072, China*

[2] *School of Electrical and Computer Engineering, Oklahoma State University, Stillwater, Oklahoma 74078, USA*

[*] *Corresponding author: gujianqiang@gmail.com*

Received December 13, 2010; accepted January 16, 2011; posted online June 29, 2011

We present a systematic study of freestanding terahertz (THz) metamaterials fabricated on Mylar film by self-aligned photolithography. THz time-domain spectroscopy (THz-TDS) transmission measurements and numerical simulations reveal the negative index of refraction in the frequency range of 0.66–0.90 THz under normal wave incidence. The observed resonance behaviors can be explained by a theoretical circuit model. The electromagnetic properties of such close-ring metamaterials are also explored in terms of geometrical parameters of the unit cell, thickness of the dielectric film, and conductivity of the close ring. This flexible metamaterial can pave the way for three-dimensional THz metamaterial fabrication and applications.

OCIS codes: 160.3918, 260.5740.
doi: 10.3788/COL20110901.S10404.

Negative index metamaterials (NIMs) have attracted enormous interest in recent years owing to their unique responses to electromagnetic radiation that are mostly lacking in natural materials[1]. Such metamaterials have become excellent platforms for demonstrating unusual electromagnetic properties, leading to unique applications, such as superlens, cloaking, antenna, and subwavelength photolithography[2−10].

The original proposal and subsequent implementation of a practical NIM composed of conventional metallic wires, split-ring resonators (SRRs), and their variations[11] have been undertaken. SRR-wire composite has been proven to be simultaneously negative in both permittivity and permeability, with overlapping electric and magnetic resonances[12]. In recent years, to improve the performance of metamaterials and to broaden their potential applications, numerous new structures have been proposed and investigated either for in-plane or normal incidence[13−20], such as fishnet[13,14], rod pairs[15], crosses[16], and "dog bones"[17−19]. In addition to these structures, close-ring resonator has recently attracted the attention of researchers for being an interesting candidate of metamaterial unit cell. In particular, the negative index has been demonstrated at far infrared in a single-ring metamaterial for in-plane incidence[21]. Compared with SRRs, close rings have two-dimensional (2D) symmetric characters and less complicated fabrication processes. However, the structure only showed a negative index at in-plane incidence[21]. Thus, it is important to exploit its resonance properties at normal incidence, which is essential for three-dimensional (3D) metamaterial and device applications.

In this letter, we present a freestanding metamaterial consisting of pairs of close rings resonating under normal wave incidence. The samples are fabricated by self-aligned photolithography on flexible dielectric polymer. With terahertz (THz) transmission measurements, comprehensive model calculation, and full-wave simulation, we demonstrate that close-ring pair (CRP) geometry exhibits a negative index of refraction at THz frequencies. Furthermore, we show that the electromagnetic response properties of the CRP structures can be controlled efficiently by varying their geometrical and material parameters.

Figure 1(a) illustrates the schematic of a CRP unit cell. An $h = 25$ μm thick isotropic Mylar film was sandwiched between an aligned pair of square close rings with a thickness of 200 nm. Under electromagnetic radiation, the opposing ring pair, as well as the adjacent rings in the same plane, formed a composite LC-resonance circuit[22]. The samples were fabricated by modified self-aligned lithography process[4]. Commercially available Mylar films were used as spacers because they possessed the quality of being transparent in both THz and visible regime. This allowed the usage of unique self-aligned photolithography fabrication. Samples with 25-μm thick Mylar spacers were freestanding and flexible; these may be useful in some applications.

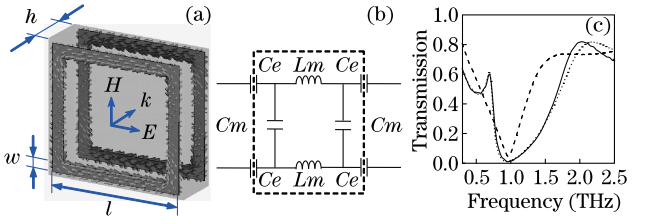

Fig. 1. (a) Schematic of a CRP unit cell with typical dimensions of l=60 μm, w=5 μm, and h=25 μm. The arrows in the rings represent surface current induced at resonance frequency. (b) Effective circuit model of the unit cell. (c) Measured (solid curve) and simulated (dotted curve) single-layer CRP metamaterial. The dashed curve illustrates the measured transmission of corresponding Al rings patterned only on one side of the Mylar.

Transmission response of CRP metamaterials was characterized under normal incidence using a photoconductive antenna-based THz time-domain spectroscopy (THz-TDS) system[23,24]. The solid curve in Fig. 1(c) shows the frequency-dependent amplitude transmission of a CRP metamaterial with d=4 μm between two adjacent rings. Compared with the ring array (dashed curve) patterned only on one side of the Mylar, CRP metamaterial revealed a new resonance peak at 0.69 THz, whereas the stop-band valley near 1.0 THz became broader. Such resonant properties were very well reproduced by numerical simulation (dotted curve). The anti-symmetric current in the ring pair, which was induced by the incident magnetic field in the dielectric spacer, together with the displacement current between them, formed a loop and resulted in negative permeability at the resonance frequency (see Fig. 1(a)). Thus, the combination of negative permittivity, indicated by the wideband valley in the transmission response of a single layer of rings (dashed curve) in Fig. 1(c), and the negative permeability may lead to a negative index of refraction near the resonance peak.

Figures 2(a) and (b) show the retrieved real and imaginary parts of the index of refraction n and the impedance z of the CRP metamaterial, respectively[16,25]. S_{11} and S_{21} parameters were obtained by the simulation of a single layer of CRP sample with 25-μm air spacers both in front of and behind it. At 0.69 and 0.76 THz, the indices of refraction approached –2.8 and –1.0, respectively.

To systematically explore the resonant behaviors of the CRP structure, we fabricated a set of CRP metamaterials with various geometrical parameters. Modification in their geometrical dimensions resulted in extensive frequency shift and amplitude modulation at the resonance (see Figs. 3(a), (c), and (e)).

According to the surface current and electromagnetic field distribution, the resonance is largely determined by two factors: magnetic response between the two sides of the CRP and the near field coupling between adjacent rings on the same side. In Fig. 1(b), we illustrate an effective circuit model of the CRP unit cell to further investigate the influence of geometrical parameters[22]. In the current study, the magnetic response was modeled by a microstrip loop across the two sides of the CRPs in the propagation direction. A coplanar line loop was used to represent the coupling between the adjacent rings at the same surface. The inductance and capacitance in the microstrips responsible for the magnetic response were denoted as $L_{\rm m}$ and $C_{\rm m}$ respectively, whereas the capacitance $C_{\rm e}$ referred to the near

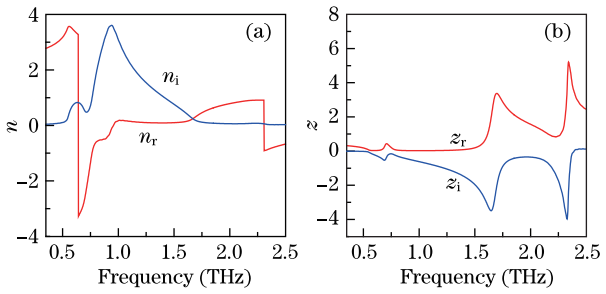

Fig. 2. Retrieved parameters of a single-layer CRP. The real and imaginary parts of the parameters are represented by the red and blue curves, respectively.

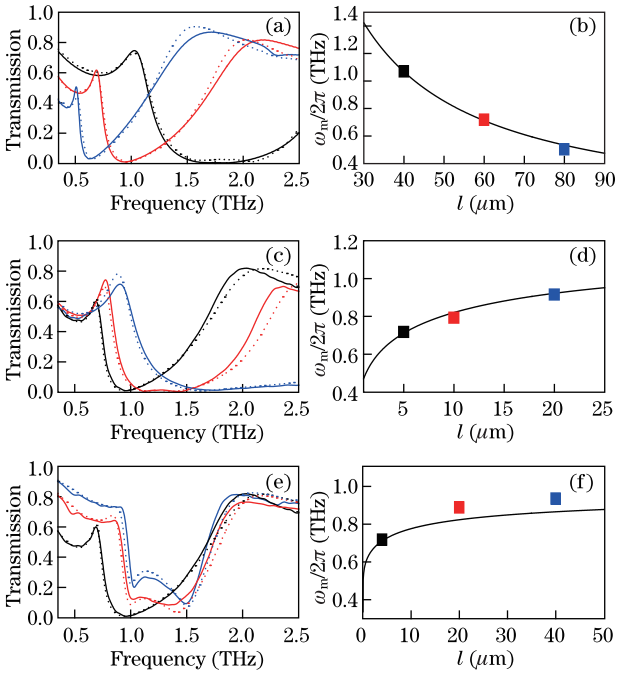

Fig. 3. (Color online) Dependence of CRP resonance on geometrical dimensions. Measured (solid curves) and simulated (dotted curves) transmissions with (a) l=40 (black), 60 (red), and 80 (blue) μm; (c) w=5 (black), 10 (red), and 20 (blue) μm; (e) d=4 (black), 20 (red), and 40 (blue) μm, respectively. (b), (d), and (f): predicted (solid curves, by the circuit model) and simulated (squares) resonance frequencies.

field coupling coefficient between the adjacent rings on the same surface. The magnetic resonance frequency can be calculated as: $\omega_{\rm m} = [L_{\rm m}(C_{\rm e}+C_{\rm m})]^{-1/2}$, with $L_{\rm m} = \mu hl/2\omega$, $C_{\rm m} = \varepsilon\omega C_1 l/h$, $C_{\rm e} = c_2 l(\varepsilon+\varepsilon_0)K\left(1-k^2\right)^{1/2}/[2K(k)]$, where ε and μ are the permittivity and permeability of the dielectric, respectively (in our case, $\varepsilon = 2.89\varepsilon_0$ and $\mu = \mu_0$); K is the first completed elliptical integration and $k = d/(d+2w)$[26]; c_1 and c_2 are two numerical factors with values between 0 and 1 representing the effective length and width of the ring arms that really take part in the resonance, respectively. The best fit for the measurements are $c_1 = 0.31$ and $c_2 = 0.11$. We compared the simulated resonance position with that predicted by the circuit model, from which we observed a reasonably good agreement (see Figs. 3(b), (d), and (f)).

Aside from the geometry of the rings, the influence of the thickness of the Mylar film and the conductivity of the metal was also investigated in the simulation. In the CST environment, we set the thickness of the Mylar film as 12.5, 25, 50, and 75 μm (see Fig. 4(a)). As the thickness increased, the transmission peak red shifted. This is the direct result of the increase on $L_{\rm m}$ and $C_{\rm m}$. Figure 4(b) shows the conductivity dependence of the CRP metamaterial. In the simulation, CRP metamaterials fabricated by silver (6.17×10^7 S/m), aluminum (3.72×10^7 S/m), brass (1.57×10^7 S/m), tin (8.7×10^6 S/m), tantalum (6.45×10^6 S/m), and lead (5×10^6 S/m) were investigated. The difference of the amplitude at the peak shown in Fig. 4(b) is quite small, with a value of only 0.06. This means that the main loss of CRP metamaterial comes from the loss in Mylar film.

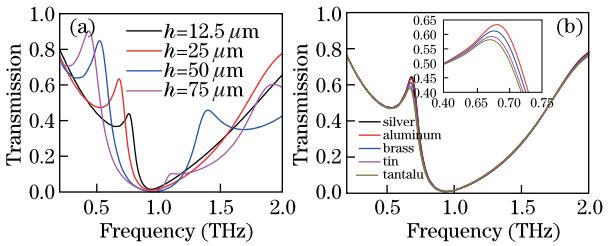

Fig. 4. (a) Influence of the thickness of the Mylar film and (b) the conductivity dependence of the CRP metamaterial.

In conclusion, we demonstrate a freestanding NIM resonating at THz frequencies, which has been fabricated using self-aligned photolithography. Experimental results have been generated using a THz-TDs, which confirmed the numerical simulations. Particular attention has been given to the impact of geometrical parameters of the proposed unit cell, the thickness of the Mylar film and the conductivity of the closed ring, on the resonant behaviors. The flexible texture, straightforward fabrication process, and interesting resonant properties of the CRP geometries are promising attributes that can help in developing 3D THz metamaterials and metamaterial-based THz components.

This work was partly supported by the U.S. National Science Foundation, the National Key Basic Research Special Foundation of China (Nos. 2007CB310403 and 2007CB310408), the National Natural Science Foundation of China (No. 60578037), and the Tianjin Sci-Tech Support Programs (Nos. 08ZCKFZC28000 and 07ZCGHHZ01100). J. Han acknowledges the financial support given by the MOE Academic Research Fund of Singapore and the Lee Kuan Yew Fund.

References

1. V. G. Veselago, Sov. Phys. Usp. **10,** 509 (1968).
2. N. Fang, H. Lee, C. Sun, and X. Zhang, Science **308,** 534 (2005).
3. D. Schurig, J. J. Mock, B. J. Justice, S. A. Cummer, J. B. Pendry, A. F. Starr, and D. R. Smith, Science **314,** 977 (2006).
4. T. J. Yen, W. J. Padilla, N. Fang, D. C. Vier, D. R. Smith, J. B. Pendry, D. N. Basov, and X. Zhang, Science **303,** 1494 (2004).
5. M. W. Klein, C. Enkrich, M. Wegener, and S. Linden, Science **313,** 502 (2006).
6. R. W. Ziolkowski and A. Erentok, IEEE Trans. Antennas Propagat. **54,** 2113 (2006).
7. H. Chen, W. J. Padilla, J. M. O. Zide, A. C. Gossard, A. J. Taylor, and R. D. Averitt, Nature **444,** 597 (2006).
8. T. Xu, Y. Zhao, J. Ma, C. Wang, J. Cui, C. Du, and X. Luo, Opt. Express **16,** 13579 (2008).
9. J. F. O'Hara, R. Singh, I. Brener, E. Smirnova, J. Han, A. J. Taylor, and W. Zhang, Opt. Express **16,** 1786 (2008).
10. R. Singh, C. Rockstuhl, C. Menzel, T. P. Meyrath, M. He, H. Giessen, F. Lederer, and W. Zhang, Opt. Express **17,** 9971 (2009).
11. B. Wood and J. B. Pendry, IEEE Trans. Microw. Theory **47,** 2075 (1999).
12. D. R. Smith, W. J. Padilla, D. C. Vier, S. C. Nemat-Nasser, and S. Schultz, Phys. Rev. Lett. **84,** 4184 (2000).
13. S. Zhang, W. Fan, K. J. Malloy, S. R. Brueck, N. C. Panoiu, and R. M. Osgood, Opt. Express **13,** 4922 (2005).
14. G. Dolling, M. Wegener, C. M. Soukoulis, and S. Linden, Opt. Lett. **32,** 53 (2007).
15. V. M. Shalaev, W. Cai, U. K. Chettiar, H. Yuan, A. K. Sarychev, V. P. Drachev, and A. V. Kildishev, Opt. Lett. **30,** 3356 (2005).
16. O. Paul, C. Imhof, B. Reinhard, R. Zengerle, and R. Beigang, Opt. Express **16,** 6736 (2008).
17. M. Awad, M. Nagel, and H. Kurz, Opt. Lett. **33,** 2683 (2008).
18. G. Donzelli, A. Vallecchi, F. Capolino, and A. Schuchinsky, Metamaterials **3,** 10 (2009).
19. A. Vallecchi, F. Capolino, and A. G. Schuchinsky, IEEE Microw. Wirel. Co. **19,** 269 (2009).
20. J. Han, J. Gu, X. Lu, M. He, Q. Xing, and W. Zhang, Opt. Express **17,** 16527 (2009).
21. Z. Hao, M. C. Martin, B. Harteneck, S. Cabrini, and E. H. Anderson, Appl. Phys. Lett. **91,** 253119(2007).
22. J. Zhou, E. N. Economon, T. Koschny, and C. M. Soukoulis, Opt. Lett. **31,** 3620 (2006).
23. D. Grischkowsky, S. Keiding, M. Exter, and C. Fattinger, J. Opt. Soc. Am. B **7,** 2006 (1990).
24. A. K. Azad, J. M. Dai, and W. Zhang, Opt. Lett. **31,** 634 (2006).
25. X. Chen, T. M. Grzegorczyk, B. Wu, J. Pacheco, and J. A. Kong, Phys. Rev. E **70,** 016608 (2004).
26. K. C. Gupta, R. Garg, and I. J. Bahl, *Microstrip Lines and Slotlines* (Artech House, Boston·London, 1979).